Proceedings of the ASME 2010 3rd Joint US-European Fluids Engineering Summer Meeting and
8th International Conference on Nanochannels, Microchannels, and Minichannels
FEDSM-ICNMM2010
August 1-5, 2010, Montreal, Canada

FEDSM-ICNMM2010-30273

HIGH RESOLUTION MEASUREMENT OF WALL TEMPERATURE DISTRIBUTION DURING FORCED CONVECTIVE BOILING IN A SINGLE MINICHANNEL

Nils Schweizer [a], Martin Freystein [a], Peter Stephan [a,b]

[a] Institute of Technical Thermodynamics
Technische Universität Darmstadt
Darmstadt, Germany
email: schweizer@ttd.tu-darmstadt.de
freystein@ttd.tu-darmstadt.de

[b] Center of Smart Interfaces
Technische Universität Darmstadt
Darmstadt, Germany
email: pstephan@ttd.tu-darmstadt.de

ABSTRACT

Cooling systems incorporating convective boiling in mini- and microchannels achieve very high thermal performance. Although many investigations related to the subject have already been conducted, the basic phenomena of the heat transfer mechanisms are not yet fully understood. The development of empirical correlations based only on flow pattern maps does not lead to a deeper knowledge of the mechanisms. In this study a comprehensive measurement technique that was successfully adapted in pool boiling experiments [8,9] was used for the investigation of forced convective boiling of FC-72 in a single rectangular minichannel. This technique allows the measurement of the local temperature with very high spatial and temporal resolution. High speed video recording was used to observe the flow inside the minichannel. The inlet Reynolds number was kept constant for the first measurements to $Re = 200$ corresponding to a hydraulic diameter of the minichannel of 800 µm. The Bond number for the proposed setup is about $Bo \approx 1.2$. Several flow pattern regimes such as bubbly flow, slug flow and partially dryout were observed for heat fluxes up to 25 kW / m². From an energy balance at each pixel element of the thermographic recordings the local transient heat flux could be calculated and compared to the flow pattern video recordings. The results of the first experiments already give an indication about the heat transfer mechanisms at different flow regimes.

1 INTRODUCTION

Boiling in mini- and microchannels has recently attracted large interest in electronic industry. The requirements for cooling systems of electronic devices have increased significantly in the last decade. Highly integrated semiconductor units generate large amounts of heat at very small length scales. Commonly, the cooling interface of these units is larger than the unit itself, thus determining its overall size. In order to overcome this drawback high heat fluxes have to be removed directly at the chip. The high performance of flow boiling in mini- and microchannels and the possibility to integrate the evaporator directly into the chip make the process very interesting for this kind of applications.

Many investigations on convective boiling in small channels have already been conducted but up to now there has been no satisfying approach to describe the heat transfer mechanisms.

Kandlikar [1] summarized investigations related to this subject and proposed three fundamental questions for researchers: 1. How does the small passage dimension affect the bubble dynamics and the two-phase flow? 2. How is the heat transfer and pressure drop affected in these channels? 3. What is the difference in performance between single and multiple parallel channels? Furthermore, he investigated the heat transfer mechanisms during flow boiling in microchannels [2]. After nucleation, the accumulated superheat in the wall leads to rapid bubble growth. The channel is quickly filled by the bubble. The main heat transfer mechanism is then defined by the moving three phase contact line at both ends of the bubble and/or by an evaporating thin liquid film which remains at the channel wall as the elongated bubble passes through which was observed by Hardt et al. [4] and Schilder et al. [12]. The scientific community still does not agree in this last point.

Nevertheless, Kandlikar states that the heat transfer mechanism is similar to that of nucleate boiling because of the dryout and rewetting processes of the wall. This statement contradicts the conclusion of Qu and Mudawar [3] who predict that annular flow is the dominant flow pattern and forced convection boiling is the dominant heat transfer mechanism for water microchannel heat sinks.

Thome et al. [11] presented a three-zone evaporation model demonstrating that the transient evaporation of the thin liquid films surrounding elongated bubbles is the dominant heat transfer mechanism, not nucleate boiling as stated by Kandlikar [2]. Assuming a constant and uniform heat flux the confined elongated bubbles are trapping a thin film of liquid between the bubble and the inner tube wall. The three zones repeat periodically and proceed as follows: 1. a liquid slug passes without any entrained bubbles; 2. an elongated bubble passes causing a thin liquid film at the inner tube wall; 3. if the thin evaporating film of the bubble dries out before the arrival of the liquid slug of the next cycle, a apour slug passes.

However, all experimental investigations up to date were focused on either flow pattern observation and/or on the evaluation of the heat transfer on a macro scale. Global heat transfer measurements were generally performed with discrete temperature sensors like thermocouples. By measuring the channel wall temperature distribution using thermochromic liquid crystals (Piasecka et al. [5], Muwanga and Hassan [6]) or infrared thermography (Diaz et al. [7]) the heat transfer coefficient was evaluated. Although the resolution of these thermography techniques is far higher than a thermocouple measurement system, the investigations were still performed on a macro scale. Since the wall thickness is in the order of hundreds of microns the temperature field is smeared due to thermal inertia and heat conduction in the wall. High frequency temperature fluctuations on a micro scale are not observable with these systems.

In order to fundamentally investigate the heat transfer mechanism during flow boiling in mini- and microchannels a thermography technique with very high spatial and temporal resolution was used. This technique was developed at the Institute of Technical Thermodynamics in Darmstadt and successfully implemented in pool boiling experiments in microgravity [8]. With this technique it is possible to measure the local temperature drop at the thin heated wall caused by a moving contact line of a growing vapour bubble. By applying the technique on flow boiling in mini- and microchannels the role of moving contact lines and thin liquid film evaporation at the channel wall could be clarified.

2 EXPERIMENTAL SETUP AND PROCEDURE

The experimental loop consists of a degasification and condenser unit, a pump and the test section as shown in Figure 1. The working fluid FC-72 is pumped by a micro annular gear pump (mzr®-2921, HNP Mikrosysteme) from the condenser to the test section. Due to the high affinity of FC-72 to dissolve noncondensable gases a continuously working degasification unit is installed to avoid effects on the boiling process. Furthermore, the degasification unit functions as a liquid reservoir for the test loop.

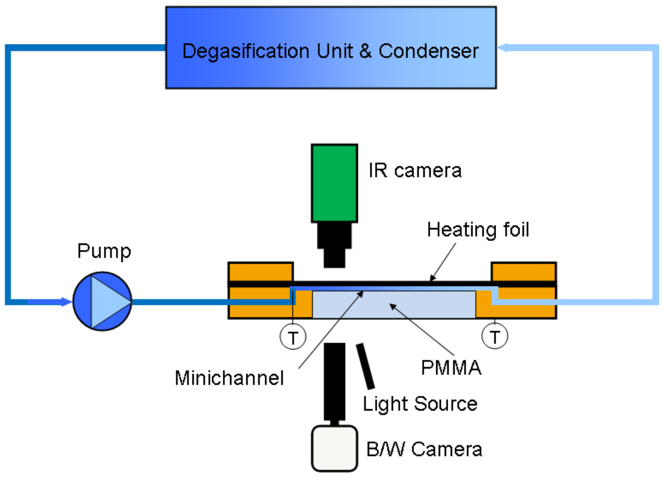

Figure 1: Schematic of test loop

The test section consists of two copper supports defining the minichannel geometry in between. The copper supports are thermally controlled by a constant temperature loop with a temperature close to the saturation temperature of FC-72 (t_{sat} = 56°C for 1 bar). This allows the assumption that the two channel walls are adiabatic and the only heat flux to the fluid during flow boiling is due to the electric heating of the steel foil. The liquid enters the test section subcooled and is heated up by the copper support close to saturation temperature before entering the heating foil area. Further downstream the evaporation starts on the heating foil. The two-phase flow exiting the minichannel is led back to the condenser.

The single rectangular minichannel (2 mm x 0.5 mm) with a length of 80 mm is manufactured into a copper block. The temperature of the lower copper support and therefore of the two sides of the channel is controlled by a constant temperature loop. The upper side of the channel is bordered by the heating foil. The foil is made of stainless steel with a thickness of 20 µm and is fixed by the thermally controlled upper copper support. The bottom of the channel is closed by an acryl glass window (PMMA) for optical access. The cross section of the test section is shown in Figure 2.

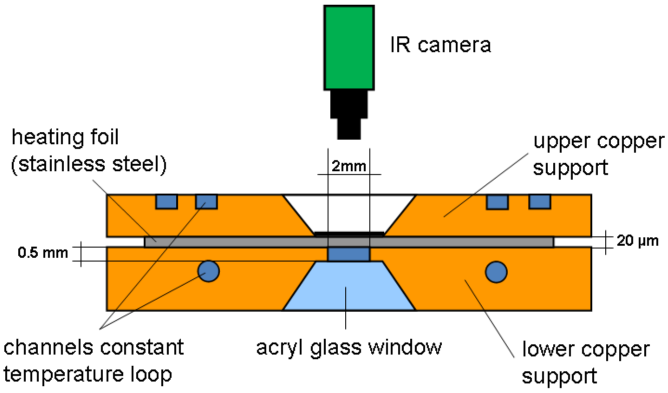

Figure 2: Schematic of the cross section of the test section

For the infrared thermography the backside of the heating foil is coated with a thin graphite layer. The foil is heated by electrical DC and therefore the copper parts are electrically and thermally insulated to the heating foil with a lacquer coating.

2.1 MEASUREMENT INSTRUMENTATION

The system pressure is measured with an absolute pressure sensor within the test section. The degasification unit and the reservoir are corresponding with the ambience so that the system pressure is at any time about 1 bar. Temperature measurements using K-type thermocouples in the liquid line from the pump to the test section and at the in- and outlet of the test section are installed to monitor the experimental conditions.

For the local temperature measurements at the graphite coated rear side of the heating foil a high speed infrared camera (Thermosensorik CMT 256 MHS, ± 0.5 K after in-situ calibration) is used with a frame rate of f = 1000 Hz and a resolution of 224 x 224 pixel. In combination with a field of view of about 6.66 mm this leads to a spatial resolution of 29.76 µm / pixel. Due to inhomogeneities of the heating foil and the graphite coating on the backside of the foil the calibration of the camera has to be made in-situ. Therefore the acryl glass window is replaced by a copper structure which is pressed on the upside of the heating foil. The temperature of the copper and the foil can now be assumed as equal and homogenous. Using the constant temperature loop the temperature of the test section is then varied in steps of 5°C over the entire measurement range. Then 400 images are recorded using experimental conditions (e.g. frame rate and field of view) to generate a raw data matrix for each temperature step. The mean temperature of the copper block is determined by calculating the average temperature of three K-type thermocouples that are implemented in the copper structure for the calibration process. Next to the in-situ calibration there is a non uniformity correction given by the manufacturer due to the different response characteristic of each pixel element of the camera chip.

For the observation of the flow pattern regimes a high speed video camera is used (X-Stream XS-3, IDT) with a frame rate of f = 1000 Hz and a resolution of 512 x 512 pixels. The high speed camera is positioned aligned with the IR-camera to allow the direct connection of flow pattern regimes and heat transfer results. A cold light source (3,000 K, 500 lm) is used to illuminate the channel for the high speed video recordings. In combination with a field of view of about 8.5 mm this leads to a spatial resolution of 16.67 µm / pixel.

2.2 DATA ANALYSIS

From the high resolution temperature fields the local heat flux distribution from the heater into the fluid q_{fluid} is calculated by a method developed by Schweizer [8]. Using a discretization algorithm like the one suggested by [10], the heating foil is divided into pixel elements dV_{HF} as shown in Figure 3.

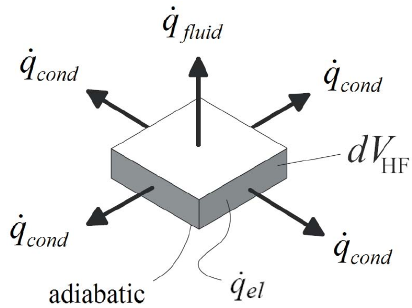

Figure 3: Energy balance of one pixel element [9]

For each pixel element of the heating foil an unsteady energy balance is applied using Fourier's equation:

$$\delta \rho c \frac{\partial T}{\partial \tau} = \lambda \left(\frac{\partial^2 T}{\partial x^2} + \frac{\partial^2 T}{\partial y^2} \right) + \dot{q}_{el} - \dot{q}_{fluid}. \qquad (1)$$

For the calculations it is assumed that the back side of the heating foil is adiabatic and that the temperature is homogenous within one pixel element. The local heat flux from the heater into the fluid can be calculated taking into account the transient heat storage in the foil material, the lateral heat conduction to adjacent pixel elements and the electrical heat flux

The electrical heat flux is the most important input value of the forced convective boiling system. Therefore, the heat flux q_{el} is calculated using only the electric current I and the foil resistance to avoid errors due to unknown contact resistances and voltage drop between the electrodes and the heating foil [9]. To eliminate the possible effect of heat conduction from the electrodes into the measurement area, the electrodes are positioned in a 25mm distance area covered by fluid. The resistance is determined by using the specific electric resistance of the foil, which is a temperature dependent material constant. The electrical heat flux is therefore

$$\dot{q}_{el} = \frac{I^2 \cdot \rho_{20}\left(1+\alpha_{20}\left(t_w - 20°C\right)\right)}{b_f^2 \cdot s_f} \quad (2)$$

where the index f is for the heating foil. The constant electric current is given by the power source with an accuracy of about 10 mA. The specific resistance is taken from literature and has for stainless steel (X5 CrNi 18 9) a value of 0.73 Ω mm²/m at 20°C. The temperature dependency of the electric resistance can be assumed with $\alpha_{20} = 0.005$ 1/K. The total estimation of the measurement error of the evaluation of the heat flux provides according to [9] for a heat flux $q_{el} = 17{,}250$ W/m² a maximum uncertainty of ± 9.4%.

$$\frac{\Delta\dot{q}_{el}}{\dot{q}_{el}} = 0.188 \quad (3)$$

The uncertainty decreases for higher and increases for lower heat fluxes (e.g. ± 21% for $q_{el} = 7{,}500$ W/m²). A detailed description of the measurement technique and error analysis can be found in [8,9].

2.3 MEASUREMENT PROCEDURE

Due to the high affinity of FC-72 to dissolve noncondensable gases the degasification unit and all components of the experimental loop need to be set to a preset value and need to run for a warm up process before each experiment to remove noncondensable gases from the system. Afterwards the pump speed is adjusted and the heat flux of the heating foil is increased to a maximum of about 25 kW / m². The measurements are then done in heat flux steps with decreasing heat flux to avoid hysteresis effects. A new data point is recorded when the system reaches steady state. The cameras are triggered to ensure synchronous sequences with a length of two seconds.

3 RESULTS AND DISCUSSION

In the present study, experiments on subcooled forced convective boiling of FC-72 were conducted. The varied parameter is the heating power. Observed flow pattern regimes as bubbly flow and slug flow are discussed. The results are presented in form of single pictures of the high speed video recordings, the temperature field recordings of the IR-camera and the calculated heat flux distribution. The flow direction is in all figures from left to right. Furthermore an analysis of the average heat flux and temperature is presented for the entire channel and as well for a cross sectional area. The horizontal lines in Figure 5 of the temperature field and the heat flux distribution represent exemplarily the two walls of the channel. The area of the heating foil beyond is already covered by the lower copper support.

3.1 BUBBLY FLOW

In the bubbly flow regime single bubbles are passing through the channel, see Figure 4. The bubbles are already confined by the height of the channel but their size is still smaller than the cross sectional area of the minichannel.

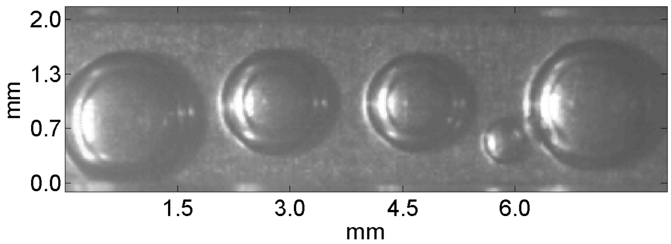

Figure 4: High speed video recording of bubbly flow for $q_{el} = 6$ kW / m² and Re = 200

After nucleating at the wall the bubbles grow rapidly into the channel while moving over the heating surface due to the forced convection. An area of high heat flux can be observed near the three phase contact line of each bubble, compare Figure 5.

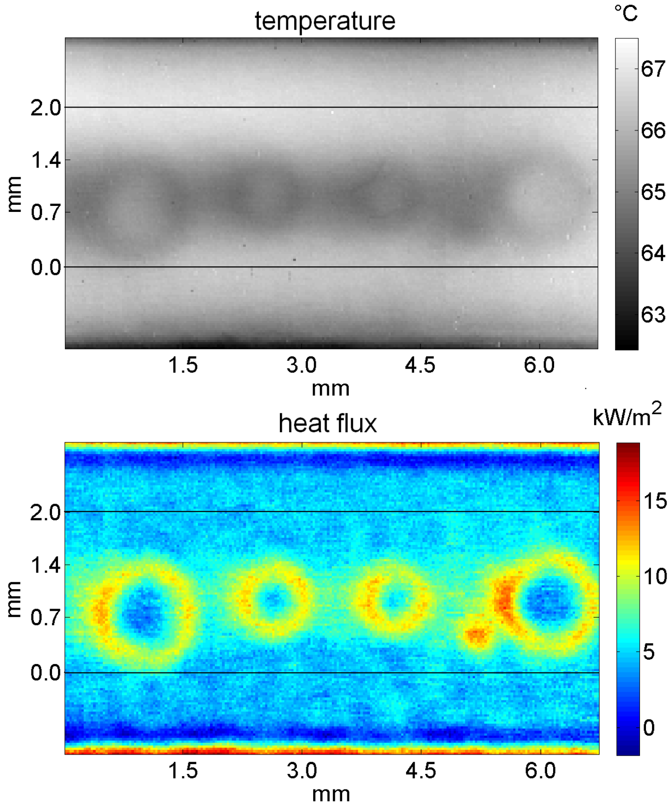

Figure 5: Temperature field and heat flux distribution for bubbly flow for $q_{el} = 6$ kW / m² and Re = 200

The wall superheat in the area of the moving three phase contact line of the bubbles is in average about 2-3 K lower compared to the areas covered by liquid only. In a two second sequence of the high speed video recordings it can be seen that bubbles close behind a large bubble are decreasing in size due to the lower wall superheat and local heat flux. The reason is that the bubble is growing into the channel and into the subcooled liquid in the middle of the channel. In this case the condensation rate at the top of the bubble in the subcooled liquid is higher than the evaporation rate at the wall. The heat flux absorbed by the previous passing bubble is not compensated by the electrical heating. The bubbles are decreasing and slowing down until the foil is heated up again. In comparison to a solid heating surface this effect is much more distinctive in the proposed experimental setup because of the very thin heating foil of 20 µm and therefore very small heat storage capacity. But a thin heater is necessary to avoid horizontal heat conduction in the foil in order to obtain sharp temperature signals on the backside of the heater for the thermographic recordings.

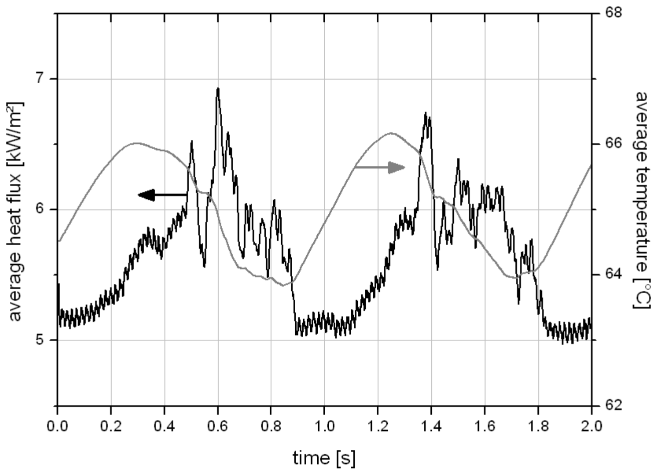

Figure 6: Average temperature and heat flux over time of the entire channel for bubbly flow for q_{el} = 6 kW / m² and Re = 200

For a recorded sequence this effect of the thin heating foil results in a sinusoidal curve progression of average temperature and heat flux signal, as shown in Figure 6. The periodic heat flux signal is time shifted to the temperature signal as expected. The wall temperature is increasing because of the constant electrical heating. As the superheat of the wall increases, evaporation starts and the average heat flux exceeds the value that can be compensated by the electrical heating. The temperature decreases due to the very small heat capacity of the foil and the next periodic cycle begins.

The average heat flux for a cross sectional area of the minichannel is shown in Figure 7. This analysis allows the detection of three phase contact line of passing bubbles. Each peak in the average heat flux corresponds with a passing bubble. The maximum values of the peaks are decreasing due to the periodic temperature signal mentioned above. The integral value of the average heat flux of about 5.8 kW / m² corresponds well to the calculated electrical heat flux of 6 kW / m².

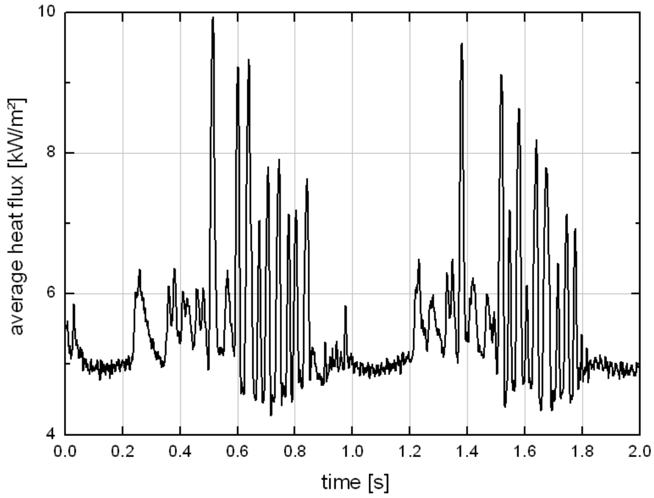

Figure 7: Average heat flux over time of a cross section of the channel for bubbly flow for q_{el} = 6 kW / m² and Re = 200

3.2 SLUG FLOW

In the slug flow regime the bubble shape is confined by the channel dimensions. The bubbles grow into the channel and rapidly reach the size of the cross sectional area. The bubble is then elongated due to further evaporation and bubble growth in flow and counter flow direction. Images of the high speed video recording of the front and back part of one typical elongated bubble are shown in Figure 8.

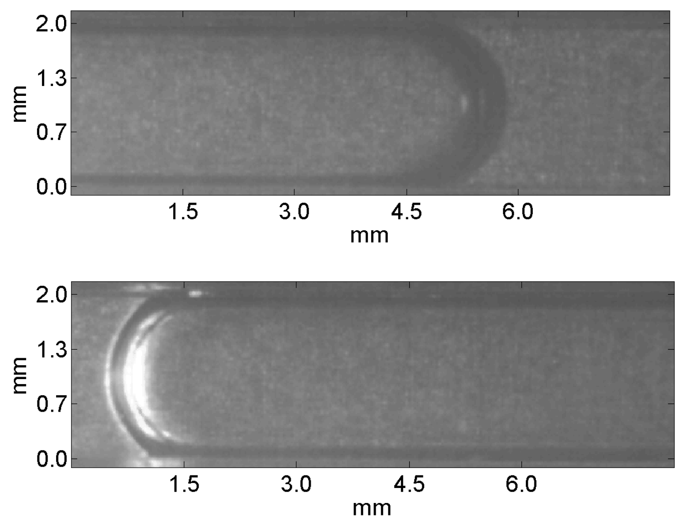

Figure 8: High speed video recording for slug flow of the front and back part of an elongated bubble for q_{el} = 7.5 kW / m² and Re = 200

Pictures of two different points in time are necessary because the length of the elongated bubble is already larger than twice the field of view.

The temperature field and the heat flux distribution for the front and back part of the elongated bubble are shown in Figures 9 and 10. The shape of the bubble can be clearly seen in both representations. The wall superheat is dropping by 5 K directly behind the three phase contact line of the bubble front and is increasing while the vapor slug of the bubble is passing, see Figure 9. The second temperature drop occurs when the three phase contact line of the back of the bubble is moving over the heated surface. The level of superheat in the vapor slug region is mainly defined by the length of the elongated bubble. For long bubbles even an increase of the superheat to values of 15 K ($t_w \approx 71°C$) was observed. At the corners of the channel the temperature is nearly constant for a passing bubble. The slight temperature increase in counter flow direction might be due to horizontal heat conduction from the higher temperature regions of the foil in the middle of the channel.

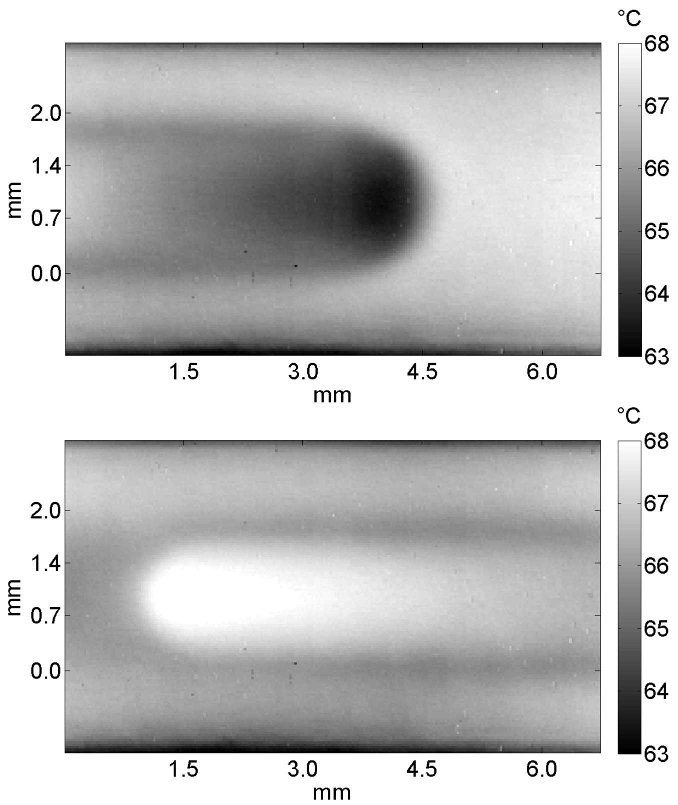

Figure 9: Temperature field for slug flow for q_{el} = 7.5 kW / m² and Re = 200

The heat flux distribution allows the identification of two areas of significantly high heat transfer, see Figure 10. As expected from the temperature field the areas are near the two moving contact lines while the heat flux at the front is about two times higher than at the back of the bubble. Near the edges of the channel walls the heat flux remains nearly constant for the passing vapor slug.

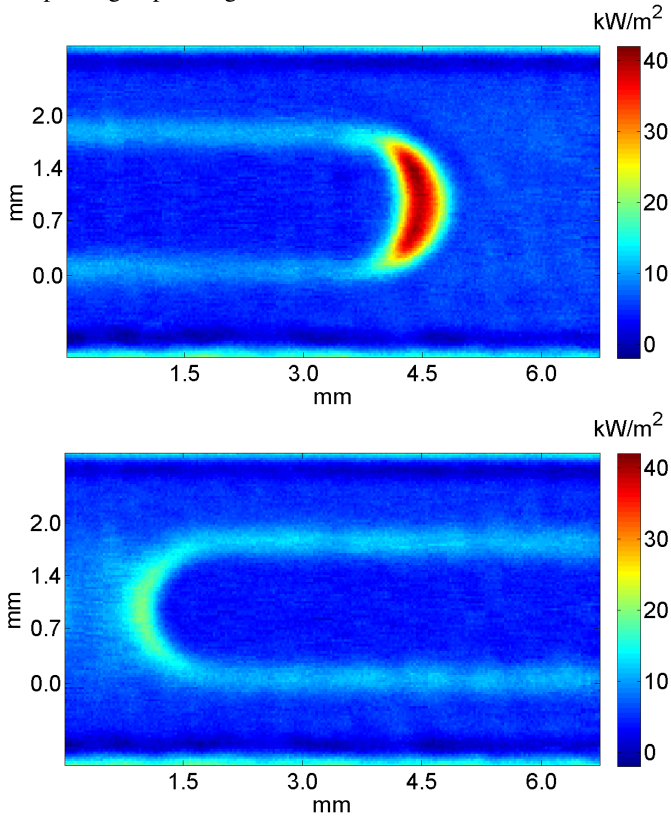

Figure 10: Heat flux distribution for slug flow for q_{el} = 7.5 kW / m² and Re = 200

There is no increase in heat flux visible for the wall area while the elongated bubble is passing. The average value of the nearly constant heat flux in this area is about 5 kW / m². The dominating influence of the thin film evaporation as proposed by Thome et al. [11] in the three-zone evaporation model can not be seen in the presented results for a single rectangular minichannel. These results indicate that the heat transport near the micro region is of great importance during forced convective boiling in minichannels. Preliminary results close to dryout of the channel support this assumption.

The average heat flux over time of the middle cross section for the slug flow regime is shown in Figure 11. The two vertically lines are marking the two positions in time when the pictures of the high speed video recording and the temperature field of the IR-camera are taken. The recording time of the picture of the just passing front is represented by the dotted line whereas the recording time of picture of the back of the elongated bubble is represented by the dashed line. The analysis of the average heat transfer allows in comparison to the bubbly flow not only the detection of a passing bubble but for the case of the elongated bubble as well the determination of a passing front and back part.

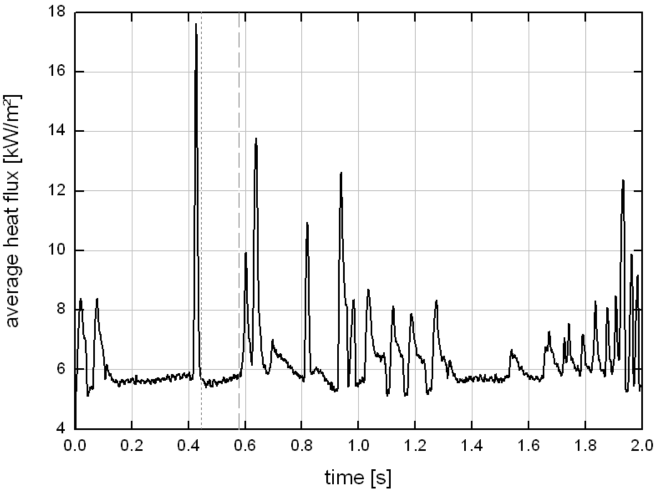

Figure 11: Average heat flux over time of a cross section of the channel for slug flow for q_{el} = 7.5 kW / m² and Re = 200

Each passing elongated bubble is represented by a large heat flux peak for the passing contact line of the bubble front followed by a second peak for the contact line of the bubble end. The second peak is about half of the size of the first one as already estimated according to Figure 10. The integral value of the average heat flux of about 7.2 kW / m² corresponds well to the calculated electrical heat flux of 7.5 kW / m².

4 CONCLUSIONS AND OUTLOOK

A comprehensive measurement technique was successfully adapted to forced convective boiling of FC-72 in a single minichannel. This technique allows the determination of the local heat flux distribution in combination with the observation of flow pattern regimes. For a constant Reynolds number of Re = 200 flow pattern regimes as bubbly and slug flow were observed for different heat fluxes. The analysis of the experimental data indicates a great influence of the heat transfer near the micro region.

The next steps will focus on an extension of the experimental conditions towards a parameter study for different heat and mass fluxes. A more detailed examination of the great difference in heat flux between advancing and receding contact line has to be done.

NOMENCLATURE

b_f	width of heating foil	[m]
c	heat capacity	[J/(kg K)]
I	electric current	[A]
p	system pressure	[Pa]
$\dot{q}_{cond}$	conductive heat flux	[W/m²]
$\dot{q}_{el}$	electrical heat flux	[W/m²]
$\dot{q}_{fluid}$	heat flux from heater to fluid	[W/m²]
s_f	thickness of heating foil	[m]
t_w	wall temperature	[°C]
t_{sat}	saturation temperature	[°C]
T	temperature	[K]

GREEK SYMBOLS

α_{20}	temperature coefficient	[1/K]
δ	thickness	[m]
∂	partial	[-]
λ	thermal conductivity	[W/(m K)]
ρ	density	[kg/m³]
ρ_{20}	electric resistivity	[Ω mm²/m]

ACKNOWLEDGMENTS

The authors would like to thank Andreas Fenner for his valuable contribution in the experimental series and the data analysis.

REFERENCES

[1] Kandlikar S.G., Fundamental issues related to flow boiling in minichannels and microchannels, Exp. Thermal and Fluid Science 26 (2002)

[2] Kandlikar S.G., Heat Transfer Mechanisms During Flow Boiling in Microchannels, Journal of Heat Transfer 126 (2004)

[3] Qu W. Mudawar I., Flow boiling heat transfer in two-phase micro-channel heat sinks – I. Experimental investigation and assessment of correlation methods, Int. J. Heat Mass Transfer 46 (2003)

[4] Hardt S., Schilder B. Tiemann D., Kolb G. Hessel V. Stephan P., Analysis of flow patterns emerging during evaporation in parallel microchannels, Int. J. Heat Mass Transfer 50 (2007)

[5] Piasecka M., Hozejowska S., Poniewski M. E., Experimental Evaluation of Flow Boiling Incipience of Subcooled Liquid in a Narrow Channel, Proc. 5th Int. Conf. Boiling Heat Transfer, Jamaica (2003)

[6] Muwanga R., Hassan I., A Flow Boiling Heat Transfer Investigation of FC-72 in a Microtube Using Liquid Crystal Thermography, J. of Heat Transfer, Vol.129 (2007)

[7] Diaz M.C., Boye H., Hapke I., Schmidt J., Staate Y., Zhekov Z., Investigation of flow boiling in narrow channels by thermographic measurement of local wall temperatures, Microfluid Nanofluid (2005)
[8] Schweizer N., Stephan P., Experimental study of bubble behaviour and local heat flux in pool boiling under variable gravitational conditions, Multiphase Science and Technology 21 (2009)
[9] Wagner E., Stephan P., High resolution measurements at nucleate boiling of pure FC-84 and FC-3284 and its binary mixtures, Journal of Heat Transfer 131 (2009)
[10] Alifanov, O., Inverse Heat Transfer Problems, Springer-Verlag, Berlin Heidelberg New York (1994)
[11] Thome J.R., Dupont V., Jacobi A.M., Heat transfer for evaporation in microchannels. Part I: presentation of the model, International Journal of Heat and Mass Transfer 47 (2004)
[12] Schilder B., Man S.Y.C., Kasagi N., Hardt S., Stephan P, Flow Visualization and Local Measurement of Forced Convection Heat Transfer in a Microtube, Journal of Heat Transfer 132 (2010)